



Cite this: *Soft Matter*, 2018, **14**, 8006

Two time scales for self and collective diffusion near the critical point in a simple patchy model for proteins with floating bonds†

J. Bleibel,^{ab} M. Habiger,^a M. Lütje,^a F. Hirschmann,^a F. Roosen-Runge,^{ib} c
 T. Seydel,^d F. Zhang,^{ib} a F. Schreiber^{ib} a and M. Oettel^{ib} *^a

Using dynamic Monte Carlo and Brownian dynamics, we investigate a floating bond model in which particles can bind through mobile bonds. The maximum number of bonds (here fixed to 4) can be tuned by appropriately choosing the repulsive, nonadditive interactions among bonds and particles. We compute the static and dynamic structure factor (intermediate scattering function) in the vicinity of the gas–liquid critical point. The static structure exhibits a weak tetrahedral network character. The intermediate scattering function shows a temporal decay deviating from a single exponential, which can be described by a double exponential decay where the two time scales differ approximately by one order of magnitude. This time scale separation is robust over a range of wave numbers. The analysis of clusters in real space indicates the formation of noncompact clusters and shows a considerable stretch in the instantaneous size distribution when approaching the critical point. The average time evolution of the largest subcluster of given initial clusters with 10 or more particles also shows a double exponential decay. The observation of two time scales in the intermediate scattering function at low packing fractions is consistent with similar findings in globular protein solutions with trivalent metal ions that act as bonds between proteins.

Received 22nd March 2018,
 Accepted 15th August 2018

DOI: 10.1039/c8sm00599k

rsc.li/soft-matter-journal

1 Introduction

Patchy particles represent an attractive model for the equilibrium and dynamical properties of protein systems.¹ One reason for their great success is that these models, on the one hand, access general soft matter properties shared by proteins but, on the other hand, are able to also adapt to the complexity of protein structure in a versatile way. Evidence for patchy interactions in protein systems is vast, starting from the general consideration of non-spherical shape and inhomogeneous surface pattern of charge and hydrophobicity. Numerical calculations based on real protein structures show that few highly attractive relative orientations dominate the protein interaction.² While the existence of the metastable liquid–liquid phase separation points to overall short-ranged attractions in the pair potential,^{3,4} the shape and location of the binodal points indicate an additional influence

of patchy attractions.^{5,6} The existence of protein crystals at relatively low packing fractions indicates the importance of patchy attractions.⁷ The notion of patches is also supported by the effects of point mutations in the protein sequence that do not alter the protein shape, but significantly vary the protein solubility and crystallization pathway.^{8–13} Patchy interactions in nature thus effectively allow for a “negative selection pressure”, as many proteins would disfavor agglomeration and crystallization.

Patchy interactions in protein solutions can also be induced or enhanced. Examples are solutions of several globular proteins in electrolytes with trivalent metal ions.^{14–22} The existence of a liquid–liquid phase separation (LLPS) and its reentrant character with changing salt concentration can be explained semiquantitatively using a colloidal model with ion-activated patches.¹⁹ Here, “empty” patches (negatively charged surface spots) become activated by the binding of a cation and may bind to a second empty patch on a different protein, *i.e.* forming an ion bridge. Indeed, ion bridges have been observed in protein crystals with multivalent cations,²³ and the cation binding to acidic residues and the resulting charge inversion have been confirmed in experiment and simulation.^{24,25} In addition to the liquid–liquid phase separation, the experimental system shows more features in the phase diagram, most notably lines away from the LLPS region in the

^a Institut für Angewandte Physik, Universität Tübingen, Auf der Morgenstelle 10, 72076 Tübingen, Germany. E-mail: martin.oettel@uni-tuebingen.de

^b Max-Planck-Institut für Intelligente Systeme, Heisenbergstr. 3, 70569 Stuttgart, Germany

^c Division for Physical Chemistry, Lund University, 22100 Lund, Sweden

^d Institut Laue-Langevin, B.P. 156, 38042 Grenoble, France

† Electronic supplementary information (ESI) available. See DOI: 10.1039/c8sm00599k

c_p – c_s plane (protein and salt concentration, respectively), which divide clear and turbid states. In static light scattering experiments at quite small protein packing fractions of a few percent, these lines show up as apparent or pseudo-spinodal lines with diverging scattering intensity.¹⁷

A general feature of attractive and charged particles is the formation of equilibrium clusters, which has been predicted by a simple argument:^{26–28} if particles exhibit a short-ranged attraction and a long-ranged (Coulomb) repulsion, single particles attach until the repulsion of the cluster is strong enough to destabilize further attachment. Computer simulations support this notion of cluster formation due to competing interactions.^{28–35} Colloidal clusters have been observed experimentally in colloidal solutions,³⁶ and predictors for structural signatures of an intermediate-range order peak have been suggested.³⁷ The nature of these clusters is not always clear, though.

As expected from this colloidal picture, clusters are also observed in protein solutions. Most prominently, the formation of equilibrium clusters was evidenced in concentrated protein solutions of lysozyme.³⁸ As reversible clustering of proteins is promising for improved drug delivery of antibodies at elevated volume fractions,³⁹ a characterization of the nature of clusters, *i.e.* static and irreversible or transient and reversible, is of great importance. For lysozyme, the combination of small-angle scattering techniques, nuclear magnetic resonance, neutron spin echo spectroscopy, and dynamic light scattering suggests that the protein clusters are rather dynamic and transient instead of static and irreversible.^{37,40–44} Similarly, β -lactoglobulin was found to form small clusters at elevated concentrations that appear static on time scales of several nanoseconds,²² but transient on longer time scales.⁴⁵ Large metastable clusters of proteins have been studied experimentally by light scattering and microscopy for various proteins such as hemoglobin, lumazine synthase, lysozyme and monoclonal antibodies.^{39,44,46–50}

In these cases, the possible degree of patchiness in the protein attractions could not be addressed, since a direct experimental signature is not obvious. A recent study suggested that patchy interactions could be addressed using the translational–rotational diffusional coupling in concentrated solutions,⁵¹ as apparent from the full dependence on volume fractions, which requires extensive experiments. A different, more pragmatic approach can be based on the expectation that for patchy particle systems in the vicinity of a liquid–vapour transition (corresponding to a LLPS on protein systems), the directional attraction is strong enough to promote the formation of (non-static) clusters. This is supported by simple mean-field arguments similar to Flory–Stockmayer theory (see *e.g.* ref. 19). Such clusters would manifest themselves in at least a second relaxation time. Indeed, in solutions of bovine serum albumin (BSA) in the presence of yttrium cations, a second relaxation time in the dynamic structure factor measured by dynamic light scattering was found,¹⁷ implying an additional channel of relaxation for long-time gradient diffusion at length scales of many protein diameters, *i.e.* at length scales of extended clusters. As a different apparent signature of clusters in the

same experimental system,²⁰ the short-time self diffusion was found to be reduced as a function of the salt/protein ratio (*i.e.* the strength of patchy attractions according to the model in ref. 19) but did not show significant deviations from a single decay on nanosecond time scales. We remark that these two limiting cases do not contradict, but complement each other (again, clusters could be rigid on the short time scales of typical neutron scattering experiments and transient on longer time scales), and further experiments as well as theoretical and simulation results are needed to provide a comprehensive multi-scale picture of cluster effects. This necessity is supported by apparent, but not comprehensively understood, cluster signatures in other experimental systems. An early study⁵² investigated the dynamic structure factor near the critical point in bovine γ_B -crystalline solutions and found the appearance of two characteristic time scales roughly differing by a factor of 10. In contrast, a recent study on the same protein stressed that both gradient diffusion around the critical point and cage diffusion on the scale of the protein diameter were consistent with a single decay,⁵³ and could be linked to the cluster formation of patchy particles, which eventually cause a dynamical arrest at comparably low volume fraction.⁵⁴ These results resemble the phenomenology of lysozyme, where clusters with an intermediate lifetime are formed with increasing volume fraction, but do not show additional relaxation phenomena.^{41,43} Based on these experimental studies, it is of importance to develop an understanding of how clusters of patchy particles would impact the experimental observables such as correlation functions probed in scattering techniques.

In this context, it is important to stress that proteins are comparably flexible, and patches might not be small spots on the surface, but rather large areas with mutual interactions. A rigid crosslinking between two proteins in fixed orientation seems improbable, which also has to be considered in the choice of the patchy model to be explored. The types of patchy models studied in the literature address these considerations differently. Models with fixed, sticky spots on the surface of particles lead to rather rigid bonds. Kern–Frenkel models⁵⁵ (with fixed conical attraction sites) allow an independent tuning of the range and the angular flexibility of bonds. On the other hand, models with floating bonds may entirely discard fixed surface positions for attraction spots. These basic types of models are discussed briefly below. Beyond these simple models, the charged nature of patches and possibly also counterions can be taken into account explicitly.^{56–58}

In this work, we choose the floating-bond type of the simple models in order to avoid an explicit and computationally demanding description of electrostatics and investigate a simple, patchy-like colloidal model that consists of particles (colloids, proteins) and bonds (binding agents such as the trivalent cations in the experiments of ref. 17). The model shows a liquid–gas phase separation (equivalent to the LLPS in protein solutions) similar to conventional patchy models.¹ We compute static and dynamic structure factors (which are quantities that are also frequently determined in experiments) and investigate their behavior close to the spinodal and the

critical points of the liquid–gas separation (which is at a particle packing fraction of about 0.1). The packing fraction is low enough for the system to be far away from the region of system-spanning network formation that would entail slowing-down and eventual dynamic arrest at gelation points. The dynamic signatures of such a network formation and arrest have been studied, *e.g.* in a sticky spot model with 4 sites, which gives rise to the formation of a random, fully connected tetrahedral network.^{59,60} There, the long-time dynamics is driven by the evolving network of metastable domains. Nevertheless, at such low packing fractions as 0.1 and below, we also find two time scales in the dynamic structure factor of the system, similar to experiments.¹⁷ An analysis of the dynamic clusters in real space also reveals the existence of two time scales. We interpret this as a particular feature of patchy models, at least of the type investigated here, which further confirms the usefulness of patchy colloidal models for the description of certain protein solutions.

The paper is organized as follows. In Section 2, the floating-bond model and the simulation methods are introduced. Results for static and dynamic structure factors and an analysis of clusters at a fixed time and their time evolution are presented in Section 3. A discussion of the obtained results in relation to experiments and further perspectives are contained in Section 4.

2 Floating-bond model and simulation methods

Simple models for patchy particles are the sticky-spot model and the Kern–Frenkel model.⁵⁵ In the sticky-spot model, point patches are located on the surface of a hard spherical colloid (with radius $\sigma/2$). Point patches interact attractively when the distance between any two patches is smaller than a patch radius $\delta/2$ ($\delta \ll \sigma$), see Fig. 1(a). In the Kern–Frenkel model, patches are modelled as spherical cones of radius $(\sigma + \delta)/2$. Any two patches interact attractively if they intersect with each other and if the vector connecting the centres of mass of the two colloids passes through both of them. The equilibrium properties of these models along with basic simulation techniques are reviewed in ref. 61. We use a model simplified even further by employing a binary model with isotropic but non-additive pairwise interactions (“floating bond model”), see Fig. 1(b). The first species represents colloids (hereafter “particles”) and the second species mediates the attractive interactions between the particles (hereafter “bonds”). The interactions between particles and bonds (outside a hard core) are attractive and short-ranged and the radius of the bonds is small. The interaction between two bonds is repulsive, however with a larger interaction radius. This prevents two bonds coming too close to each other and limits the maximum number of bonds that can bind to the surface of a particle (see Fig. 1(c)). The model was introduced and its static properties studied by Zaccarelli and coworkers,⁶² employing hard potentials for the particle–particle and bond–bond interactions and a square-well interaction

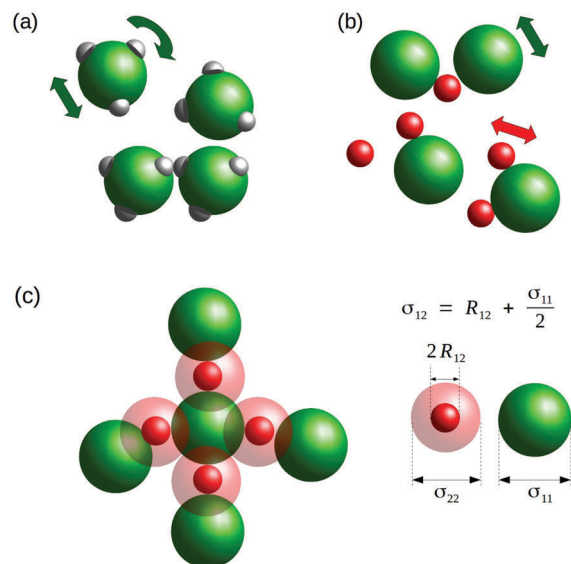


Fig. 1 (a) Schematic simple patchy particle model, a one component system of particles (green) with mutually attractive patches (grey) and thus anisotropic interactions. The particles have translational and orientational degrees of freedom, visualized by the dark green arrows. (b) “Floating bond model”, a binary system of particles and bonds. Attractive interactions only exist between particles and bonds, all interactions can be chosen as isotropic. Particles (green) and bonds (red) have translational degrees of freedom only (dark green and red arrows, respectively). (c) In the floating-bond model, realized with hard interactions, σ_{12} is independent from σ_{11} and σ_{22} . The size of σ_{22} (transparent red sphere, larger than $2R_{12}$) prevents the possibility of more than 4 bonds binding to a particle (green sphere).

for the particle–bond interaction. Some dynamic properties (using event-driven molecular dynamics) have been studied subsequently in ref. 63.

Experimental protein systems (such as those with globular proteins in trivalent salt solutions) possess features of patchy particle models with fixed patches (specific surface groups) and of the floating-bond model (mobile cations). Concerning the numerical treatment, the particular choice of the “floating bond model” has some advantages: all particles are symmetric with respect to rotational degrees of freedom. This renders simulations fast and thus allows for rather simple numerics and large systems. Below, we will introduce a version of the floating-bond model with continuous potentials, which can be treated using Brownian dynamics.

2.1 Model potentials

According to ref. 62, the restriction to a maximum of 4 bonds per particle and 2 particles per bond can be approximately realized with the choice of hard sphere diameters $\sigma_{22} = 0.8\sigma_{11}$ and $\sigma_{12} = 0.55\sigma_{11}$ (see Fig. 1(c)). Although a fifth bond is theoretically possible, it practically never occurs if the square-well interaction range δ between particles and bonds is chosen to be small ($\delta = 0.03\sigma_{12}$ in ref. 62). We adopted the following continuous form of the potentials $u_{ij}(r)$ (with $i, j = 1, 2$), which closely approximates the hard and square well potentials of ref. 62:

$$\begin{aligned}
 u_{ii}(r) &= \begin{cases} 4\epsilon_{ii} \left[\left(\frac{d_{ii}}{r}\right)^{12} - \left(\frac{d_{ii}}{r}\right)^6 + \frac{1}{4} \right] & (r < 2^{1/6} d_{ii}) \\ 0 & (r > 2^{1/6} d_{ii}) \end{cases} \\
 u_{12}(r) &= \begin{cases} 4\epsilon_{12} \left[\left(\frac{d_{12}}{r}\right)^{12} - \left(\frac{d_{12}}{r}\right)^6 \right] & (r < 2^{1/6} d_{12}) \\ -\frac{\epsilon_{12}}{2} \left[1 + \cos\left(\frac{2\pi r'}{\lambda}\right) \right] & \left(0 < r' < \frac{\lambda}{2}\right) \\ (r' = r - 2^{1/6} d_{12}) & \\ 0 & \left(r' > \frac{\lambda}{2}\right) \end{cases} \quad (1)
 \end{aligned}$$

The hard interactions have been replaced by the repulsive part of the (shifted) Lennard-Jones potential. The Lennard-Jones diameters have been fixed by the Barker-Henderson recipe evaluated for $T \rightarrow 0$, which gives $d_{ij} = 2^{-1/6} \sigma_{ij}$. The attractive well has been replaced by a half-period cosine where the integrated strength (for $T \rightarrow 0$) of the resulting attractive well is equal to the original square well. For $\delta = 0.03\sigma_{12}$, this gives $\lambda/d_{12} \approx 0.134$. For simplicity, we chose $\epsilon_{11} = \epsilon_{22} = \epsilon_{12} =: \epsilon$ and the temperature will be measured in units of ϵ : $k_B T/\epsilon \rightarrow T$. The resulting potentials are depicted in Fig. 2.

2.2 Simulation methods

We implemented Brownian dynamics using the standard position Langevin equation⁶⁴ and the dynamic Monte-Carlo (MC) method.^{65,66} In each MC step of the dynamic MC method, small translational, random moves in the range $[-\delta l, \delta l]$ (for each cartesian direction and for all particles and bonds) are attempted and they are accepted with an average acceptance ratio a (for particles). Let D_0 be the diffusion constant for a free particle, then the time per MC sweep can be defined as

$$\delta t = \frac{\delta l^2 a}{6D_0} \quad (2)$$

This δt is independent of δl if the latter is chosen to be not too large. A dimensionless time (for later use) is defined by setting $tD_0/\sigma_{11}^2 \rightarrow t$ where $t = 1$ corresponds to the average time for an isolated particle to diffuse over a distance given by its diameter (Brownian self-diffusion time). Results on the dynamic structure factor and the cluster time evolution below were obtained with the dynamic MC method only but results for diffusion in dilute systems and for the static structure factor were obtained by simulations using both the position Langevin equation and dynamic MC. We typically simulated $N_1 = 1000$ particles and a variable number N_2 of bonds. The relative concentration of bonds is denoted by $c_b = N_2/N_1$, and the packing fraction of particles is denoted by $\Phi = (\pi\sigma_{11}^3 N_1)/(6L^3)$, where L is the side length of the cubic simulation box.

Pressure isotherms using the virial method⁶⁴ were calculated to check the location in the phase diagram (see below). The static particle-particle structure factor was calculated

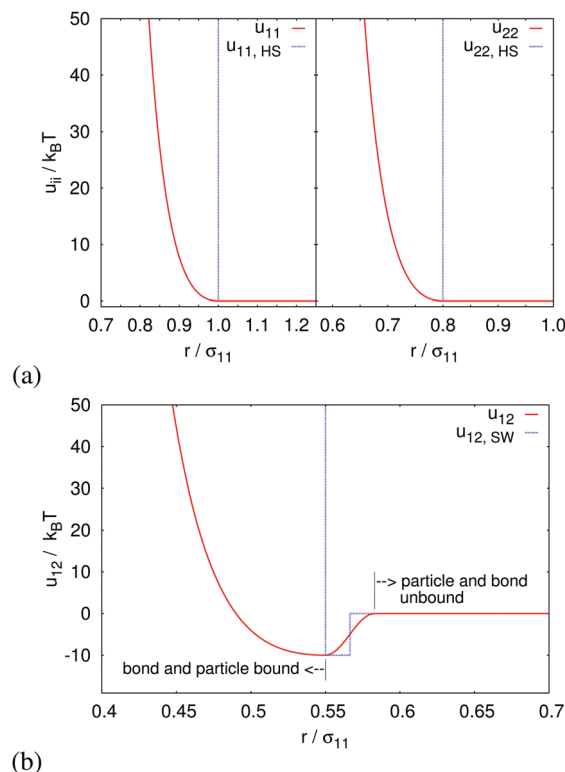


Fig. 2 The interaction potentials (in units of $k_B T$ at a reduced temperature of 0.1) in the floating-bond model. (a) Particle-particle and bond-bond interactions, dashed lines indicate the hard sphere (HS) potentials of ref. 62 and 63. (b) Particle-bond interactions, dashed lines indicate the square well (SW) potentials of ref. 62 and 63. For later use, we define bound bond-particle pairs if $r < \sigma_{12}$ occurs at some time instant and we define the breakup of a bound pair if $r > \sigma_{12} + \lambda/2$ occurs at a later time instant, where r is the center-center distance of a bond and a particle (see Section 2.2).

according to the definition

$$S(q) = \frac{1}{N_1} \left\langle \sum_{i=1}^{N_1} \sum_{j=1}^{N_1} \exp(i\mathbf{q} \cdot (\mathbf{r}_i - \mathbf{r}_j)) \right\rangle \quad (3)$$

where the sums only run over particle indices. Likewise, the self and the distinct parts of the dynamic structure factor (intermediate scattering function) were calculated according to the definition⁶⁷

$$\begin{aligned}
 S_s(q, t) &= \frac{1}{N_1} \left\langle \sum_{i=1}^{N_1} \exp(i\mathbf{q} \cdot (\mathbf{r}_i(t) - \mathbf{r}_i(0))) \right\rangle \\
 S_d(q, t) &= \frac{1}{N_1} \left\langle \sum_{i=1}^{N_1} \sum_{j(\neq i)=1}^{N_1} \exp(i\mathbf{q} \cdot (\mathbf{r}_i(t) - \mathbf{r}_j(0))) \right\rangle. \quad (4)
 \end{aligned}$$

For the purpose of calculating statistics of clusters of bonded particles and bond lifetimes, we defined connected and disconnected bond-particle pairs as indicated in Fig. 2. The gap (distances for which bond-particle pairs appear as neither connected nor disconnected) was chosen with the following idea: a connected bond (established when $r < \sigma_{12}$) becomes disconnected only when $r > \sigma_{12} + \lambda/2$. This avoids the appearance of artificially short bond lifetimes through tiny

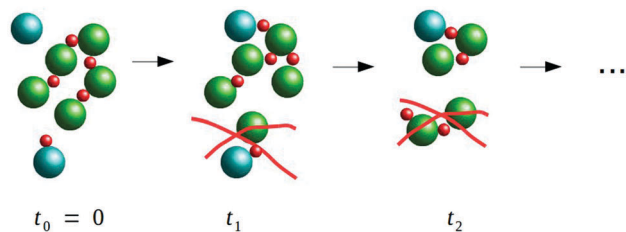


Fig. 3 Dynamic behavior of clusters: an initial cluster was identified at $t = 0$ (green particles). At the next time instance t_1 , all clusters were identified that still contained any of the initial particles and possible new particles (in blue) but only the largest cluster of these was retained for analysis at the next time instance t_2 . A new particle–bond connection is considered to be formed when particles and bonds are separated by $r < \sigma_{12}$ but an existing particle–bond connection is considered to be broken only when $r > \sigma_{12} + \lambda/2$ (see Fig. 2).

MC moves for bonds/particles when they are located close to the potential minimum of $u_{12}(r)$. For a cluster analysis, we consider two particles as directly bonded when they share a bond that is bound to each particle. The DBSCAN algorithm⁶⁸ was used to identify clusters of bonded particles. The dynamic behaviour of clusters was characterized *via* the evolution of initial clusters at time zero *via* their largest subclusters at later times (see Fig. 3).

2.3 Phase diagram

In ref. 62 and 63, several static and dynamic properties of the model with hard potentials and a maximum number of bonds equal to 4 have been studied for the bond concentration $c_b = 2$ (which can be considered as optimal for binding since in the ground state, all particles are bound and all bonds are used). As can be expected for a patchy model, the region of gas–liquid phase separation is shifted to a smaller packing fraction Φ and lower temperature T compared to a simple isotropic liquid. From the measurement of the spinodal points, the location of the critical point can be estimated as $T_c \approx 0.1$ and $\Phi_c \approx 0.1$. Near the critical point, the pressure isotherms of our floating-bond model with continuous potentials are similar. We could determine spinodal points reliably only for packing fractions $\Phi > \Phi_c$, and these are close to the results of ref. 62 (see Fig. 4).

Ref. 62 and 63 identified an “optimal network region” for $\Phi > 0.23$ and $T \lesssim T_c$. For $\Phi = 0.25$ and $T \approx 0.07$, the authors observed an arrest in time in the mean-square displacement, which points to a gel transition. Near the critical point, self diffusion is slowed down compared to very dilute systems but the system stays far from gelation.

3 Simulation results

With the information from the phase diagram at hand, we chose two paths with termination points close to the critical point (path I) and close to a spinodal point (path II, see also Fig. 4). On these paths we evaluated the static and dynamic structure of the system through the intermediate scattering function. For path I, the optimal bond concentration is chosen for binding ($c_b = 2$), the particle packing fraction is approximately the critical one

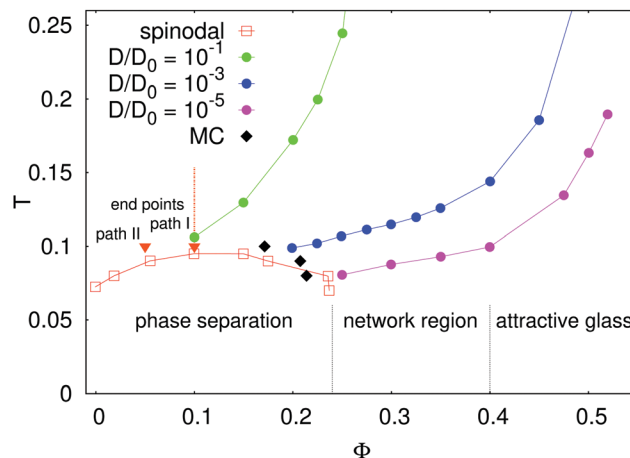


Fig. 4 Phase diagram of the model for $c_b = 2$. Open red squares are spinodal points determined in ref. 62 using hard and square well potentials. Black filled diamonds are spinodal points (obtained by fitting van der Waals loops to the pressure data) from our MC simulations using continuous potentials. Lines connecting filled circles are iso-self-diffusivity lines from ref. 63. The static and dynamic structures in this work are determined along path I (dashed line) and path II (end point shown at $\Phi = 0.05$, $T = 0.1$). Along path II, c_b is increased from 0 to 2.

($\Phi = 0.1 \approx \Phi_c$), and the temperature is lowered towards $T = 0.1 \approx T_c$. For path II, the temperature is set to approximately the critical one ($T = 0.1 \approx T_c$), the particle packing fraction is $\Phi = 0.05$ and the bond concentration is increased from 0 to the optimal one. We focus on small packing fractions $\Phi \leq \Phi_c$ and deliberately avoid the percolating network region, which has been analyzed in ref. 63 through long-time self-diffusivity. For these small packing fractions, self diffusion is still fast enough that any formed clusters and networks are highly dynamic objects.

3.1 Static structure factor

We have computed the static structure factor along paths I and II and the results are shown in Fig. 5. For path I, the effect of decreasing T towards the critical point results in an enhancement of $S(q \rightarrow 0)$. For path II, the packing fraction is quite low ($\Phi = 0.05$) and the bond concentration c_b is varied from 0 to 2. At $c_b = 0$, the system is a pure repulsive-sphere system with a weak maximum in $S(q)$ around $q\sigma_{11} \approx 6$. With increasing c_b , the maximum shifts towards $q\sigma_{11} \approx 8$ and the near-critical enhancement $S(q \rightarrow 0)$ is also clearly visible. The first maximum at $q\sigma_{11} \approx 8$ is seen for the end points of both paths. In ref. 62, higher packing fractions in the network region were studied and a similar peak together with a secondary peak at $q\sigma_{11} \approx 5$ was observed and attributed to the formation of a tetrahedrally coordinated network. At the low packing fractions studied here, the network is not fully formed and the secondary peak is hardly discernible. Snapshots near the critical point confirm this, and an example is shown in Fig. 6.

3.2 Dynamic structure factor (intermediate scattering function)

We have computed the self/distinct part of the intermediate scattering function $S_{s/d}(q, t)$ along paths I and II for various $q\sigma_{11}$

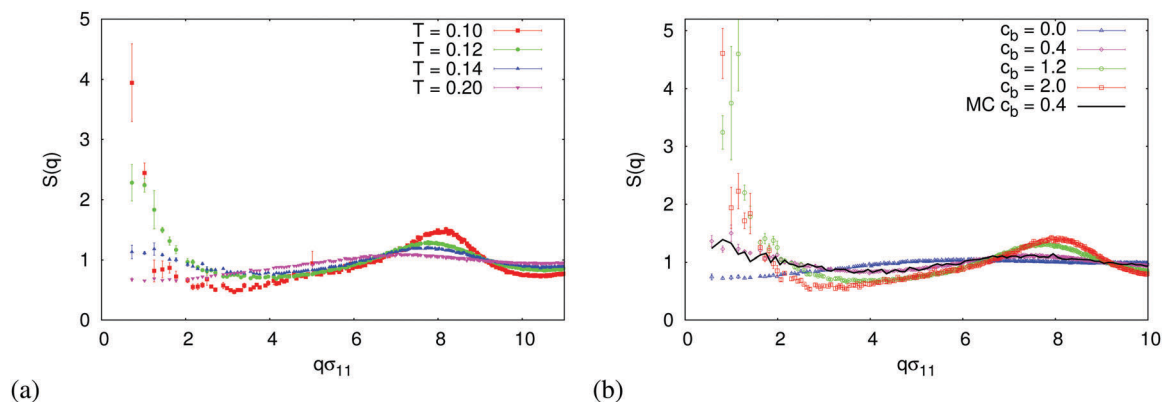


Fig. 5 Static structure factors along path I (a) and path II (b), computed using the position Langevin equation. Results agree with dynamic MC, and an example is shown in the right panel (full black line).

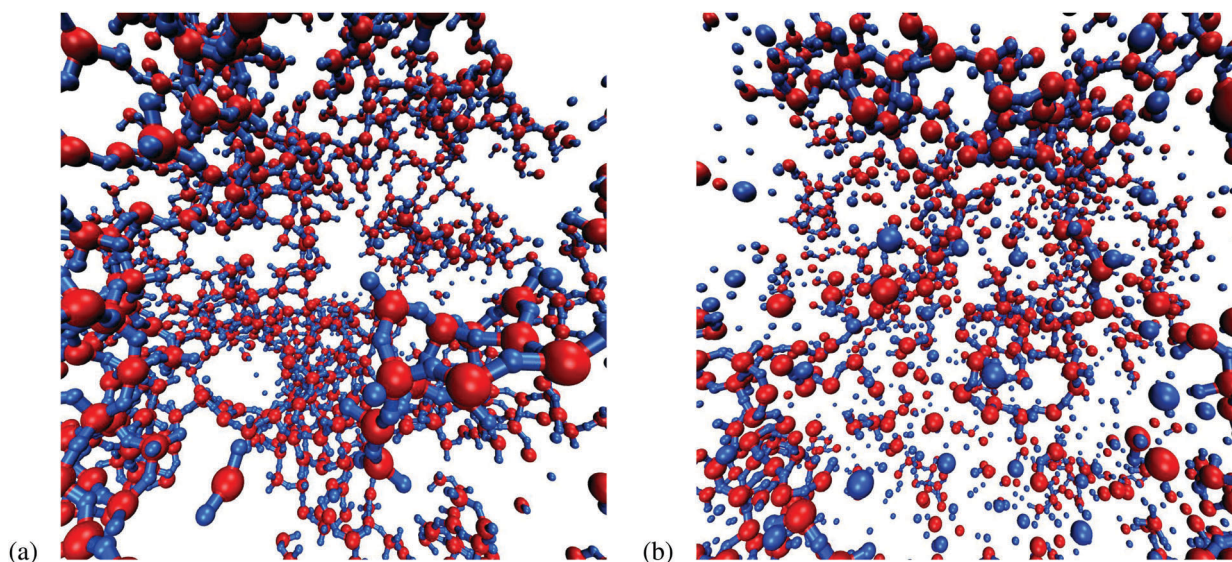


Fig. 6 (a) Snapshot at the end point of path I at $\Phi = 0.1$, $T = 0.1$ and $c_b = 2$. The system consists of clusters that themselves are a loose network. (b) Snapshot at the end point of path II at $\Phi = 0.05$, $T = 0.1$ and $c_b = 2$. Clusters are smaller and there are more unbound particles. Larger red spheres are particles and bonds are smaller blue spheres. Both particles and bonds are reduced in size such that the links (indicating connected particle–bond pairs) are more visible. Both snapshots were taken with the VMD software.⁶⁹

between 2 and 10 and reduced times between 10^{-4} and 10^2 . To exemplify these numbers, consider the experimental system of ref. 17 (BSA solutions with $\sigma \approx 70 \text{ \AA}$ and $D_0 \approx 6.3 \text{ \AA}^2 \text{ ns}^{-1}$ (no salt)). There, the self-diffusion time would be $\approx 800 \text{ ns}$ and therefore the time-range considered in the simulations corresponds to the range $0.08 \text{ ns} \dots 80 \text{ \mu s}$. The considered wave numbers correspond to $0.3 \dots 1.5 \text{ nm}^{-1}$.

In general, the statistical fluctuations in the distinct part $S_d(q,t)$ (for fixed t) differed a lot and in an unsystematic manner between different q values. We used 16 independently equilibrated systems from which we generated in total 48 trajectories for $S_{s/d}(q,t)$ at a given state point. Time was binned logarithmically with 4 stencils per decade.

Examples of the normalized structure factors (intermediate scattering functions) $f_s(q,t) = S_s(q,t)$ and $f_d(q,t) = S_d(q,t)/S(q,0)$ for $q\sigma_{11} = 4.22$ (path I) and $q\sigma_{11} = 3.68$ (path II) are shown in Fig. 7. One can see clearly that for both paths, the dynamics

becomes slower when going towards the critical point (red full squares) and the curves deviate more and more from a simple exponential decay. We captured this by fitting $f_{s/d}(q,t)$ using two exponentials:

$$f_{s/d}(q,t) = \sum_{i=1}^2 A_i^{s/d}(q) \exp(-q^2 D_i^{s/d}(q)t) \quad (5)$$

where $A_i^{s/d}(q)$ are q -dependent amplitudes and $D_i^{s/d}(q)$ are q -dependent diffusion coefficients (D_i^s for self diffusion and D_i^d for collective diffusion). This is similar to analysis of experimental data, *e.g.* in ref. 17 where (collective) diffusion coefficients (from $f_d(q \rightarrow 0, t)$) in protein–salt solutions have been analyzed approaching a spinodal-like line in the phase diagram. The fits are shown with full lines in Fig. 7 and capture the behavior of $f_{s/d}(q,t)$ rather well. Single exponential fits would deviate considerably.

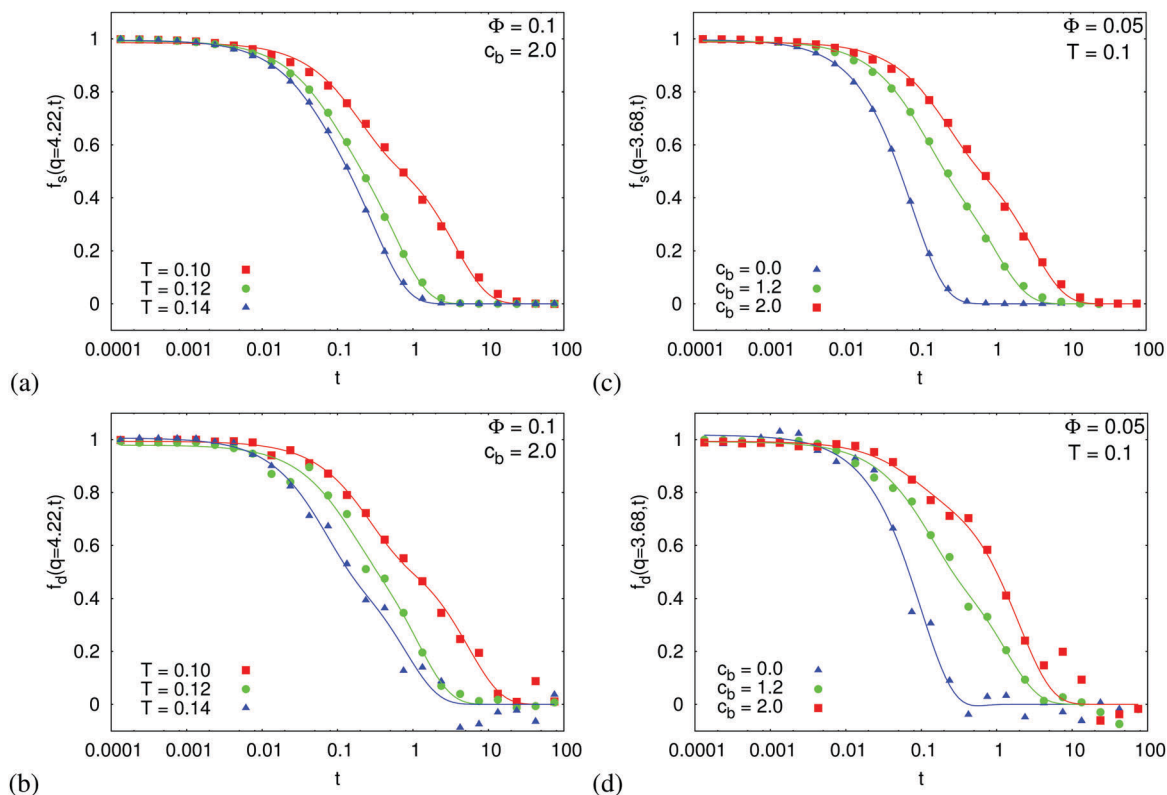


Fig. 7 Intermediate scattering functions $f_{s/d}(q, t)$ along path I ($q\sigma_{11} = 4.22$, (a) and (b)) and along path II ($q\sigma_{11} = 3.68$, (c) and (d)). The sequence blue triangles \rightarrow green points \rightarrow red squares corresponds to an approach to the terminal point of each path (critical point for path I resp. spinodal point for path II). Symbols are simulation data and lines and fits according to eqn (5).

We performed double exponential fits to all values in the indicated q range. The results for those diffusion coefficients that could be determined with an accuracy of 50% and better are collected in the ESI.† The main conclusion from the fits is that a robust separation of time scales exists over the whole q range (except for the system with no bonds on path II).

In Fig. 8, we show the error-weighted average (over q) diffusion coefficients $\bar{D}_i^{s/d}$ for path I. $\bar{D}_1^{s/d}$ (“slow” diffusion) and $\bar{D}_2^{s/d}$ (“fast” diffusion) differ by roughly one order of magnitude. Both decrease for $T \rightarrow 0.1$, *i.e.* towards the critical point, the dynamics becomes slower. The ratio becomes bigger when approaching the critical point. We note that D_1^s and D_1^d (“slow” diffusion) seem to converge towards the critical point, *i.e.* there is no difference between the time scales for self and collective diffusion for the slow process.

In Fig. 9, we show the error-weighted average diffusion coefficients for path II. As for path I, both $\bar{D}_1^{s/d}$ (“slow” diffusion) and $\bar{D}_2^{s/d}$ (“fast” diffusion) decrease for $c_b \rightarrow 2$, *i.e.* towards the spinodal line and their magnitudes differ by roughly one order of magnitude. Note however that for $c_b = 0$, there is no real slow diffusion since the system consists of purely repulsive spheres. At the end point of path II there is still a difference between the diffusion coefficients of self and collective diffusion for the slow process but we also note that this end point ($T = 0.1$, $\Phi = 0.05$, $c_b = 2$) is near the spinodal line but not so close to the critical point (see Fig. 4).

We see the same trends for collective diffusion in the experiments of ref. 17. There, the trivalent salt ions act as bonds and upon increasing the salt concentration towards the spinodal line, a similar decrease of D_i^d is observed as well as the ratio D_1^d/D_2^d of about one order of magnitude. Note that the experiments were carried out with dynamic light scattering and allow the extraction of diffusion coefficients for $q \rightarrow 0$, a limit that cannot be properly reached in the simulations.

3.3 Cluster analysis

In order to obtain more insight into the properties of the system in real space, we performed a cluster analysis. Instantaneous clusters were determined as described in Section 2.2. Along path I, we determined a normalized distribution $f(n)$ of clusters with n particles, which is shown in Fig. 10(a). When changing the reduced temperature from 0.12 to 0.1, a considerable stretching of the cluster size distribution is observed, with no maximum at a favoured cluster size. This is similar to the cluster size distribution derived from Flory–Stockmayer theory (see the example in ref. 19). Near the critical point ($T = 0.1$), we investigated the dependence of the cluster radius of gyration on the particle number, $r_g(n)$. Compact clusters would entail $r_g \propto n^B$ with $B = 1/3$, but we found $B \approx 0.43$ (see Fig. 10(b)). This points to open clusters and is corroborated by the snapshot in Fig. 6.

Time evolution of clusters was investigated using the concept of the “evolution of the largest subcluster”, see Section 2.2 and Fig. 3.

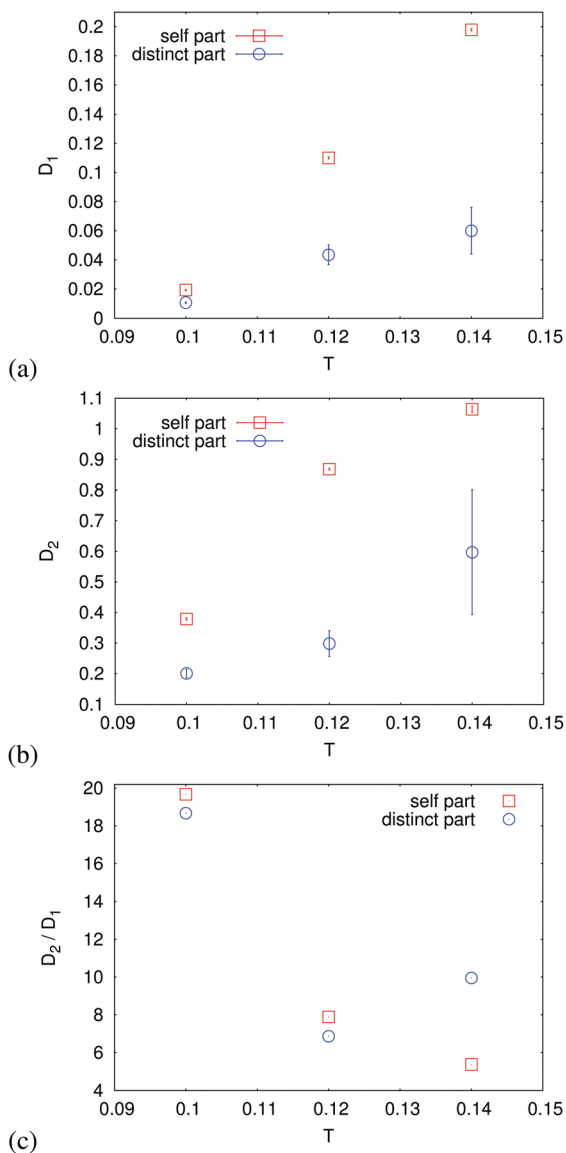


Fig. 8 Average diffusion coefficients along path I from error-weighted diffusion coefficients, which in turn are obtained from fits of the intermediate scattering functions to eqn (5). (a) Slow component. (b) Fast component. (c) Ratio between “fast” and “slow” average diffusion coefficients. Error bars are obtained from the standard deviation of the fit coefficients.

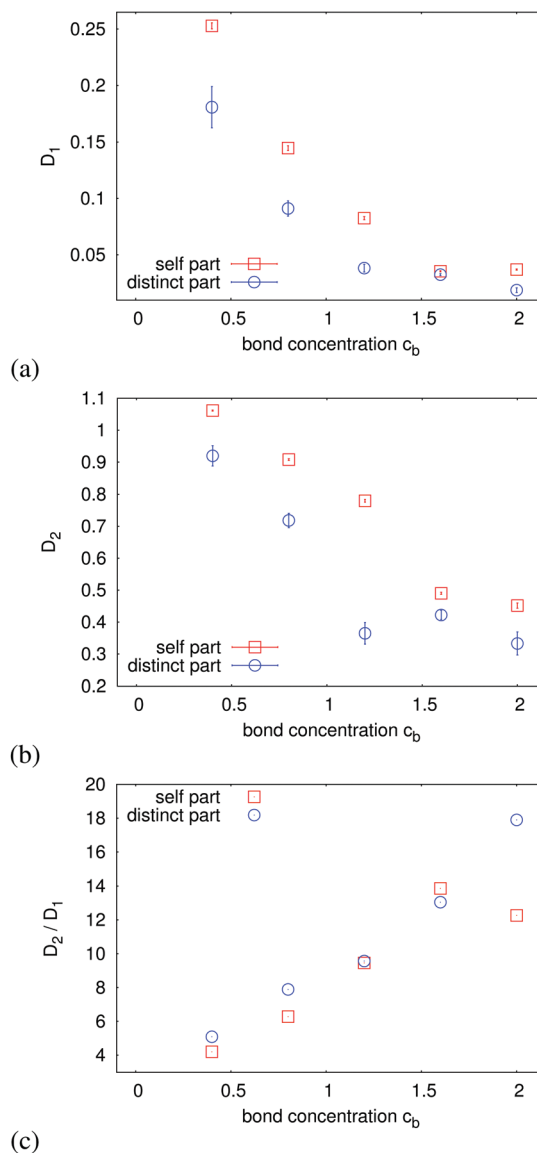


Fig. 9 Average diffusion coefficients along path II from error-weighted diffusion coefficients, which in turn are obtained from fits of the intermediate scattering functions to eqn (5). (a) Slow component. (b) Fast component. (c) Ratio between “fast” and “slow” average diffusion coefficients. Error bars are obtained from the standard deviation of the fit coefficients.

We considered only initial clusters with size $n \geq 10$. A time-dependent normalized cluster size $h(t)$ was then defined through

$$h(t) = \text{Average} \left(\frac{\text{size of the largest subcluster at time } t}{\text{size of the initial cluster}} \right). \quad (6)$$

For the end point of path II, the result for $h(t)$ is shown in Fig. 11. The time-dependence of $h(t)$ clearly shows two different time scales, which we identified by a fit to the function

$$h(t) = \sum_{i=1}^2 a_i \exp(-d_i t) + c \quad (7)$$

whose result is shown by the continuous line in Fig. 11. The two rate constants were determined as $d_1 = 0.013$ and $d_2 = 1.1$. The occurrence of two distinct time scales (as in the intermediate scattering functions) is striking but a straightforward connection of the q -dependent self and collective diffusion coefficients $D_i^{s/d}(q)$ to the rate constants d_i is not obvious. In order to obtain $h(t)$, an averaging over different cluster sizes and thus different length scales was performed whereas the intermediate scattering function allows diffusion to be extracted on a particular length scale $2\pi/q$. The rate d_2 belongs to a “fast” process occurring on the time scale of the Brownian self-diffusion time. This time scale is also similar to single-bond lifetimes, *i.e.* average lifetimes for connections between particles and bonds.

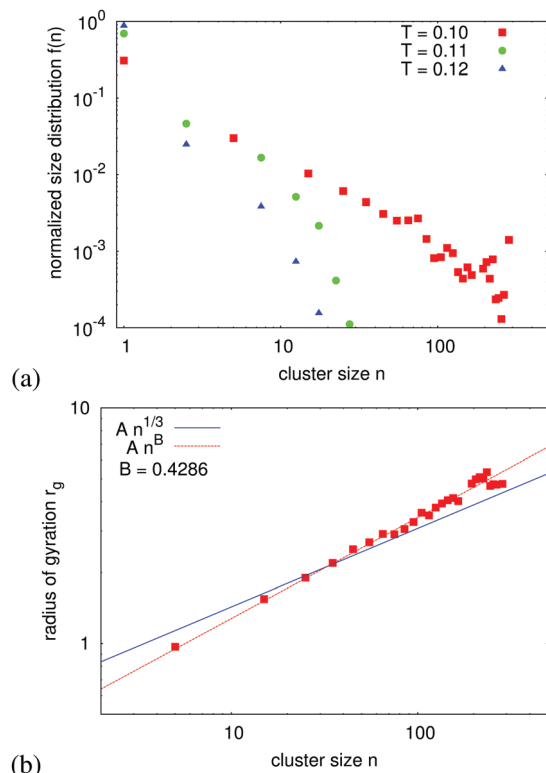


Fig. 10 (a) Normalized instantaneous size distribution for clusters (state points on path I). (b) Cluster radius of gyration vs. particle number in the cluster for the end point of path I (close to the critical point). Full lines are power laws: the fit to the data gives a coefficient of 0.43, which is larger than a power law with a coefficient of 1/3, appropriate for compact clusters.

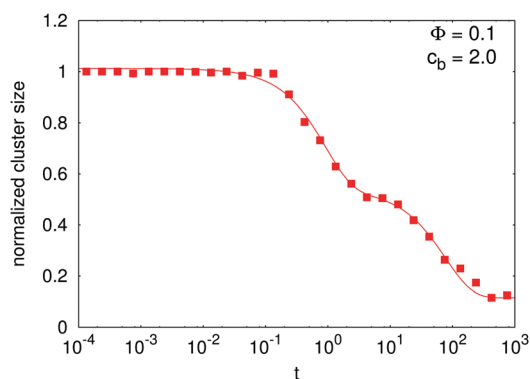


Fig. 11 Time-dependent normalized cluster size $h(t)$ for the end point of path II ($T = 0.1$, $\Phi = 0.05$, $c_b = 2$). Symbols are simulation averages and the line is a fit to eqn (7) with rate constants $d_1 = 0.013$ and $d_2 = 1.1$.

We found that in the vicinity of the spinodal line, they are on the order of 1 (e.g. on path I, they change from ≈ 0.5 at $T = 0.14$ to ≈ 3 at $T = 0.1$). Thus, the fast process in the decay of the cluster size is associated with the breakup of single bonds, which is reasonable. On the other hand, we have no clear picture of which precise mechanism is responsible for the “slow” process that occurs on a time scale of about 100 Brownian self-diffusion times. This will be subject to further investigations in the future.

From our results, we clearly infer that clusters in the vicinity of the spinodal line are highly dynamic objects, and there is no sign of a dynamical arrest for the small packing fractions investigated ($\Phi = 0.05$ and 0.1). This is in accordance with the findings of ref. 63 on self-diffusivity (see the corresponding isolines in Fig. 4). At these packing fractions, even near the critical point, there is no strong slowing-down as seen in the optimal network region ($0.25 < \Phi < 0.4$ and $T < 0.1$).

4 Conclusion and outlook

Using Brownian dynamics simulations, we studied a simple patchy model (floating-bond model) where the patchiness of particles is realized *via* a second species of bonds, which may bind to particles through a short-ranged attractive interaction. A limited, tunable valence of particles is possible by choosing an appropriate repulsion between the bonds. The model shows a shifted gas–liquid transition (typical for patchy models) as well as a network fluid and glass region.^{62,63} We have computed static and dynamic structure factors for state points approaching the critical point and the spinodal line of the gas–liquid transition. Near the spinodal and the critical points, the dynamic structure factor shows clear deviations from a decay with a single relaxation time scale. The results can be described well with the assumption of a second time scale that is about 10 times slower. In real space, near the critical point, the system shows the formation of rather open (noncompact) clusters whose size is broadly distributed. Studying the evolution of the largest subcluster of a given initial cluster also shows the existence of two time scales. The fast one can be attributed to the lifetime of connections between particles and bonds whereas the interpretation of the slow one is not obvious.

The model studied here can be viewed as a very basic description of the patchiness in the character of the effective protein–protein interactions seen in ref. 14–22. There, bonds are trivalent cations. The experimental system exhibits spinodal-like lines for rather low protein packing fractions of a few percent. Upon approaching these, the dynamic structure factor also exhibits two time scales with a ratio of about 10. The results of our model suggest that the appearance of a second time scale already at low protein packing fractions (in the simulations: 5 and 10 percent) is linked to the patchiness of the effective interactions. Within the simple model, however, the second time scale cannot be linked to a characteristic diffusion time of clusters of a particular size. The instantaneous cluster size distribution of the model near the critical point shows an onset of a power law and it does not show a peak for a specific cluster size. The clusters are transient and the second time scale in the decay of the largest subcluster points to a collective process not related to the diffusion of whole clusters.

In the experimental system of ref. 14–22, the effective protein–protein interactions also include repulsive charge–charge interactions. In the vicinity of the spinodal-like lines, the effective charge changes sign. Therefore, near this point of charge reversal, the system displays a subtle interplay of patchy

attractions and longer-ranged repulsions. There are a number of studies of systems with isotropic short-range attractions and longer-ranged repulsions^{28–35} (as alluded to in the Introduction) since these systems form stable cluster phases. Also, in these stable cluster phases, individual clusters are not long-time stable, see ref. 35 for a recent, detailed investigation. For patchy short-range attractions and longer-ranged repulsions, the implications for the phase diagram have been studied in ref. 70 and possible cluster phases identified. The connection of such cluster phases and their dynamics to the experimental system will be the subject of further study. Future simulations and theoretical studies on more refined models including longer-ranged repulsions provide the groundwork for predicting and numerically calculating experimentally accessible scattering functions. In this way, a direct comparison of the patchy colloid models with both coherent and incoherent scattering experiments will be possible based on simulations. This approach complements the analytical implementation of theoretical scattering functions for direct experimental data fitting, in particular in cases where the latter approach is not available due to the absence of analytical descriptions.

Conflicts of interest

There are no conflicts to declare.

Acknowledgements

The authors thank DFG and ANR for funding through the joint DFG-ANR project “ImmunoglobulinCrowding” (DFG SCHR 700/28-1, ANR-16-CE92-0009).

References

- 1 E. Bianchi, R. Blaak and C. N. Likos, *Phys. Chem. Chem. Phys.*, 2011, **13**, 6397–6410.
- 2 B. L. Neal, D. Asthagiri, O. D. Velev, A. M. Lenhoff and E. W. Kaler, *J. Cryst. Growth*, 1999, **196**, 377–387.
- 3 G. Foffi, G. D. McCullagh, A. Lawlor, E. Zaccarelli, K. A. Dawson, F. Sciortino, P. Tartaglia, D. Pini and G. Stell, *Phys. Rev. E: Stat., Nonlinear, Soft Matter Phys.*, 2002, **65**, 031407.
- 4 F. Platten, N. E. Valadez-Pérez, R. Castañeda-Priego and S. U. Egelhaaf, *J. Chem. Phys.*, 2015, **142**, 174905.
- 5 H. Liu, S. K. Kumar and F. Sciortino, *J. Chem. Phys.*, 2007, **127**, 084902.
- 6 C. Gögelein, G. Nägele, R. Tuinier, T. Gibaud, A. Stradner and P. Schurtenberger, *J. Chem. Phys.*, 2008, **129**, 085102.
- 7 J. P. K. Doye, A. A. Louis, I.-C. Lin, L. R. Allen, E. G. Noya, A. W. Wilber, H. C. Koke and R. Lyus, *Phys. Chem. Chem. Phys.*, 2007, **9**, 2197.
- 8 J. J. McManus, A. Lomakin, O. Ogun, A. Pande, M. Basan, J. Pande and G. B. Benedek, *Proc. Natl. Acad. Sci. U. S. A.*, 2007, **104**, 16856–16861.
- 9 A. K. Buell, G. G. Tartaglia, N. R. Birkett, C. A. Waudby, M. Vendruscolo, X. Salvatella, M. E. Welland, C. M. Dobson and T. P. J. Knowles, *ChemBioChem*, 2009, **10**, 1309–1312.
- 10 D. Fusco and P. Charbonneau, *Phys. Rev. E: Stat., Nonlinear, Soft Matter Phys.*, 2013, **88**, 012721.
- 11 N. Dorsaz, L. Fillion, F. Smallenburg and D. Frenkel, *Faraday Discuss.*, 2012, **159**, 9–21.
- 12 D. Fusco, J. J. Headd, A. De Simone, J. Wang and P. Charbonneau, *Soft Matter*, 2014, **10**, 290–302.
- 13 S. Whitelam, *Phys. Rev. Lett.*, 2010, **105**, 088102.
- 14 F. Zhang, M. W. A. Skoda, R. M. J. Jacobs, S. Zorn, R. A. Martin, C. M. Martin, G. F. Clark, S. Weggler, A. Hildebrandt, O. Kohlbacher and F. Schreiber, *Phys. Rev. Lett.*, 2008, **101**, 148101.
- 15 F. Zhang, S. Weggler, M. J. Ziller, L. Ianeselli, B. S. Heck, A. Hildebrandt, O. Kohlbacher, M. W. A. Skoda, R. M. J. Jacobs and F. Schreiber, *Proteins*, 2010, **78**, 3450–3457.
- 16 F. Zhang, R. Roth, M. Wolf, F. Roosen-Runge, M. W. A. Skoda, R. M. J. Jacobs, M. Sztucki and F. Schreiber, *Soft Matter*, 2012, **8**, 1313–1316.
- 17 D. Soraruf, F. Roosen-Runge, M. Grimaldo, F. Zanini, R. Schweins, T. Seydel, F. Zhang, R. Roth, M. Oettel and F. Schreiber, *Soft Matter*, 2014, **10**, 894.
- 18 F. Zhang, F. Roosen-Runge, A. Sauter, M. Wolf, R. M. J. Jacobs and F. Schreiber, *Pure Appl. Chem.*, 2014, **86**, 191–202.
- 19 F. Roosen-Runge, F. Zhang, F. Schreiber and R. Roth, *Sci. Rep.*, 2014, **4**, 7016.
- 20 M. Grimaldo, F. Roosen-Runge, M. Hennig, F. Zanini, F. Zhang, M. Zamponi, N. Jalarvo, F. Schreiber and T. Seydel, *J. Phys. Chem. Lett.*, 2015, **6**, 2577–2582.
- 21 O. Matsarskaia, M. K. Braun, F. Roosen-Runge, M. Wolf, F. Zhang, R. Roth and F. Schreiber, *J. Phys. Chem. B*, 2016, **120**, 7731–7736.
- 22 M. K. Braun, M. Wolf, O. Matsarskaia, S. Da Vela, F. Roosen-Runge, M. Sztucki, R. Roth, F. Zhang and F. Schreiber, *J. Phys. Chem. B*, 2017, **121**, 1731–1739.
- 23 F. Zhang, G. Zocher, A. Sauter, T. Stehle and F. Schreiber, *J. Appl. Crystallogr.*, 2011, **44**, 755–762.
- 24 F. Roosen-Runge, B. S. Heck, F. Zhang, O. Kohlbacher and F. Schreiber, *J. Phys. Chem. B*, 2013, **117**, 5777–5787.
- 25 E. Jordan, F. Roosen-Runge, S. Leibfarth, F. Zhang, M. Sztucki, A. Hildebrandt, O. Kohlbacher and F. Schreiber, *J. Phys. Chem. B*, 2014, **118**, 11365–11374.
- 26 J. Groenewold and W. K. Kegel, *J. Phys. Chem. B*, 2001, **105**, 11702–11709.
- 27 J. Groenewold and W. K. Kegel, *J. Phys.: Condens. Matter*, 2004, **16**, S4877.
- 28 F. Sciortino, S. Mossa, E. Zaccarelli and P. Tartaglia, *Phys. Rev. Lett.*, 2004, **93**, 055701.
- 29 F. Carlsson, M. Malmsten and P. Linse, *J. Phys. Chem. B*, 2001, **105**, 12189–12195.
- 30 S. Mossa, F. Sciortino, P. Tartaglia and E. Zaccarelli, *Langmuir*, 2004, **20**, 10756–10763.
- 31 P. Kowalczyk, A. Ciach, P. Gauden and A. Terzyk, *J. Colloid Interface Sci.*, 2011, **363**, 579–584.

- 32 E. Spohr, B. Hribar and V. Vlachy, *J. Phys. Chem. B*, 2002, **106**, 2343–2348.
- 33 T. Jiang and J. Wu, *Phys. Rev. E: Stat., Nonlinear, Soft Matter Phys.*, 2009, **80**, 021401.
- 34 A. Fierro, T. Abete, A. Coniglio and A. de Candia, *J. Phys. Chem. B*, 2011, **115**, 7281–7287.
- 35 S. Das, J. Riest, R. G. Winkler, G. Gompper, J. K. G. Dhont and G. Nägele, *Soft Matter*, 2018, **14**, 92.
- 36 P. N. Segrè, V. Prasad, A. B. Schofield and D. A. Weitz, *Phys. Rev. Lett.*, 2001, **86**, 6042–6045.
- 37 Y. Liu, L. Porcar, J. Chen, W.-R. Chen, P. Falus, A. Faraone, E. Fratini, K. Hong and P. Baglioni, *J. Phys. Chem. B*, 2011, **115**, 7238–7247.
- 38 A. Stradner, H. Sedgwick, F. Cardinaux, W. C. K. Poon, S. U. Egelhaaf and P. Schurtenberger, *Nature*, 2004, **432**, 492–495.
- 39 K. P. Johnston, J. A. Maynard, T. M. Truskett, A. U. Borwankar, M. A. Miller, B. K. Wilson, A. K. Dinin, T. A. Khan and K. J. Kaczorowski, *ACS Nano*, 2012, **6**, 1357–1369.
- 40 A. Stradner, F. Cardinaux and P. Schurtenberger, *J. Phys. Chem. B*, 2006, **110**, 21222–21231.
- 41 L. Porcar, P. Falus, W.-R. Chen, A. Faraone, E. Fratini, K. Hong, P. Baglioni and Y. Liu, *J. Phys. Chem. Lett.*, 2009, **1**, 126–129.
- 42 S. Barhoum and A. Yethiraj, *J. Phys. Chem. B*, 2010, **114**, 17062–17067.
- 43 F. Cardinaux, E. Zaccarelli, A. Stradner, S. Bucciarelli, B. Farago, S. U. Egelhaaf, F. Sciortino and P. Schurtenberger, *J. Phys. Chem. B*, 2011, **115**, 7227–7237.
- 44 Y. Li, V. Lubchenko and P. G. Vekilov, *Rev. Sci. Instrum.*, 2011, **82**, 053106.
- 45 R. Piazza and S. Iacopini, *Eur. Phys. J. E: Soft Matter Biol. Phys.*, 2002, **7**, 45–48.
- 46 W. Pan, O. Galkin, L. Filobelo, R. L. Nagel and P. G. Vekilov, *Biophys. J.*, 2007, **92**, 267–277.
- 47 W. Pan, P. G. Vekilov and V. Lubchenko, *J. Phys. Chem. B*, 2010, **114**, 7620–7630.
- 48 O. Gliko, N. Neumaier, W. Pan, I. Haase, M. Fischer, A. Bacher, S. Weinkauff and P. G. Vekilov, *J. Am. Chem. Soc.*, 2005, **127**, 3433–3438.
- 49 O. Gliko, W. Pan, P. Katsonis, N. Neumaier, O. Galkin, S. Weinkauff and P. G. Vekilov, *J. Phys. Chem. B*, 2007, **111**, 3106–3114.
- 50 E. Yearley, P. Godfrin, T. Perevozchikova, H. Zhang, P. Falus, L. Porcar, M. Nagao, J. Curtis, P. Gawande, R. Taing, I. Zarraga, N. Wagner and Y. Liu, *Biophys. J.*, 2014, **106**, 1763–1770.
- 51 M. Roos, M. Ott, M. Hofmann, S. Link, E. Rössler, J. Balbach, A. Krushelnitsky and K. Saalwächter, *J. Am. Chem. Soc.*, 2016, **138**, 10365–10372.
- 52 B. M. Fine, J. Pande, A. Lomakin, O. O. Ogun and G. B. Benedek, *Phys. Rev. Lett.*, 1995, **74**, 198.
- 53 S. Bucciarelli, L. Casal-Dujat, C. D. Michele, F. Sciortino, J. Dhont, J. Bergholtz, B. Farago, P. Schurtenberger and A. Stradner, *J. Phys. Chem. Lett.*, 2015, **6**, 4470.
- 54 S. Bucciarelli, J. S. Myung, B. Farago, S. Das, G. A. Vliegthart, O. Holderer, R. G. Winkler, P. Schurtenberger, G. Gompper and A. Stradner, *Sci. Adv.*, 2016, **2**, e1601432.
- 55 N. Kern and D. Frenkel, *J. Chem. Phys.*, 2003, **118**, 9882.
- 56 A. Abrikosov, B. Stenqvist and M. Lund, *Soft Matter*, 2017, **13**, 4591.
- 57 R. Hieronimus, S. Raschke and A. Heuer, *J. Chem. Phys.*, 2016, **145**, 064303.
- 58 M. A. Blanco and V. K. Shen, *J. Chem. Phys.*, 2016, **145**, 155102.
- 59 L. Rovigatti and F. Sciortino, *Mol. Phys.*, 2011, **109**, 2889.
- 60 S. Roldan-Vargas, L. Rovigatti and F. Sciortino, *Soft Matter*, 2017, **13**, 514.
- 61 L. Rovigatti, J. Russo and F. Romano, *Eur. Phys. J. E: Soft Matter Biol. Phys.*, 2018, **41**, 59.
- 62 E. Zaccarelli, F. Sciortino and P. Tartaglia, *J. Chem. Phys.*, 2007, **127**, 174501.
- 63 C. Mayer, F. Sciortino, R. Tartaglia and E. Zaccarelli, *J. Phys.: Condens. Matter*, 2010, **22**, 104110.
- 64 M. P. Allen and D. J. Tildesley, *Computer simulation of liquids*, Oxford University Press, Oxford, 1987.
- 65 L. Berthier and W. Kob, *J. Phys.: Condens. Matter*, 2007, **19**, 205130.
- 66 E. Sanz and D. Marenduzzo, *J. Chem. Phys.*, 2010, **132**, 194102.
- 67 J.-P. Hansen and I. McDonald, *Theory of simple liquids*, Academic Press, London, 3rd edn, 2006.
- 68 M. Ester, H.-P. Kriegel, J. Sander and X. Xu, *Kdd*, 1996, **96**, 226.
- 69 W. Humphrey, A. Dalke and K. Schulten, *J. Mol. Graphics*, 1996, **14**, 33.
- 70 D. Stopper and R. Roth, *Eur. Phys. J. E: Soft Matter Biol. Phys.*, 2017, **96**, 042607.